EPJ Web of Conferences **95**, 03032 (2015)
DOI: 10.1051/epjconf/20159503032

Recent results from CMS

Robert Schöfbeck[1,a] on behalf of the CMS collaboration

[1] *Institute of High Energy Physics, Austrian Academy of Sciences, Nikolsdorfergasse 18, 1050 Vienna*

Abstract. The CMS experiment at the Large Hadron Collider at CERN collected a dataset of 19.5fb^{-1} during 8 TeV proton-proton operation. A large number of groundbreaking results were obtained from the analysis of this dataset, among them the discovery of the Higgs boson and precision measurements of important Standard Model parameters, for example the mass of the top quark. Subtle processes like the production of a Z boson by fusion of two W bosons have been measured for the first time. Moreover, many searches for physics beyond the Standard model have been carried out, both in the context of supersymmetry and beyond, which often provide tight constraints in model parameter space. This brief summary is a a short overview of the most important recent CMS results at 7 and 8 TeV.

1 Introduction

Since the start of the LHC proton-proton operation in 2010, the Compact Muon Solenoid (CMS) detector has been operating with increasing efficiency. The initial center-of-mass energy of $\sqrt{s} = 7$ TeV was raised in 2012 to $\sqrt{s} = 8$ TeV. The peak instantaneous luminosity of $7.5 \cdot 10^{33}$ cm^{-2} s^{-1} approached the design value of 10^{34} cm^{-2} s^{-1}, ensuing 20 to 50 simultaneous interactions per bunch crossing (pile-up). The resulting challenge for event reconstruction was met by sophisticated algorithms and calibration procedures designed to mitigate effects from pile-up. These allowed to keep the detector performance approximately constant over the full data-taking period. In total, CMS accumulated a total of 19.5 fb^{-1} at $\sqrt{s} = 8$ TeV.

Using this high quality dataset, the Higgs boson was discovered as first announced jointly by the ATLAS and CMS experiments on July 4$^{\text{th}}$, 2012. This milestone completes one of the major goals of the LHC experiments and establishes the mechanism that generates the masses of elementary particles in the Standard Model (SM). One focus of the CMS experiment therefore are precision measurements in the Higgs sector, where deviations from the SM might help uncover the origin of electroweak symmetry breaking. In parallel with the new particle discovery, the CMS experiment has kept expanding our knowledge of frontier particle physics with several new precision measurements of electroweak physics observables and of the properties of the top quark. Furthermore, a rich physics programme is carried out in order to test models of physics beyond the SM, comprising searches for supersymmetry and many more exotic theories.

This document is organized as follows. Section 2 describes briefly the experimental environment. The final results of the 8 TeV data taking period on properties of the Higgs boson are reviewed in

[a] e-mail: robert.schoefbeck@cern.ch

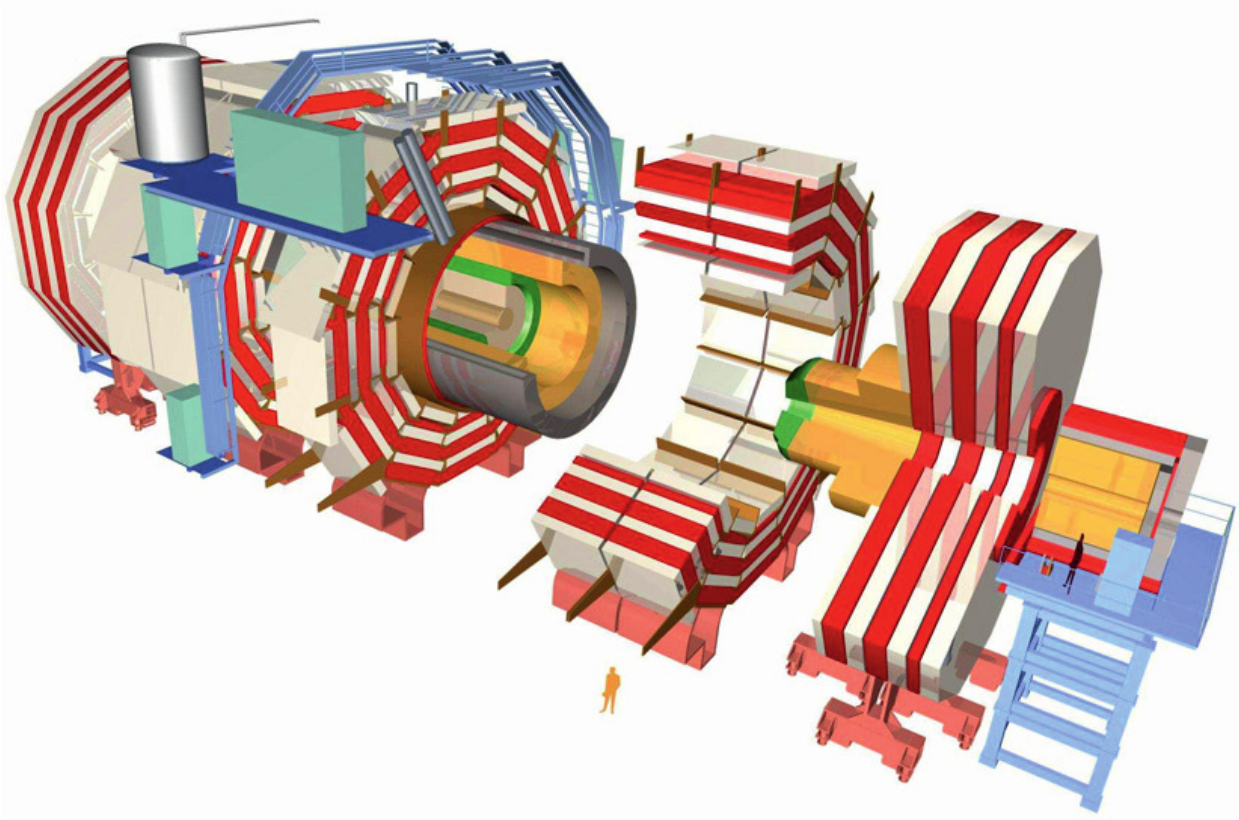

Figure 1. An overview of the CMS detector, showing the outer muon chambers (white) embedded in iron (red), the calorimeter system (ECAL, in green, and HCAL, in orange) and the tracker in the core of the central barrel.

Sec. 3. Recent precision measurements of the strong coupling constant, in the electro-weak sector and of the top quark mass are described in Sec. 4. Finally, a summary on results of supersymmetry is given in Sec. 5.

2 The CMS detector and event reconstruction

CMS uses a right-handed coordinate system in which the z axis points in the anticlockwise beam direction, the x axis points towards the center of the LHC ring, and the y axis points up, perpendicular to the plane of the LHC ring. The azimuthal angle ϕ is measured in the x-y plane, and the polar angle θ is measured with respect to the z axis.

The CMS superconducting solenoid, 12.5 m long with an internal diameter of 6 m, provides a uniform magnetic field of 3.8 T. The inner tracking system is composed of a pixel detector with three barrel layers at radii between 4.4 and 10.2 cm and a silicon strip tracker with 10 barrel detection layers extending outwards to a radius of 1.1 m. This system is complemented by two endcaps, extending the acceptance up to $|\eta| = 2.5$. The momentum resolution for reconstructed tracks in the central region is about 1% at $p_{\mathrm{T}} = 100\,\mathrm{GeV}/c$. The calorimeters inside the magnet coil consist of a lead tungstate crystal electromagnetic calorimeter (ECAL) and a brass-scintillator hadron calorimeter (HCAL) with coverage up to $|\eta| = 3$. The quartz/steel forward hadron calorimeters extend the calorimetry coverage up to $|\eta| = 5$. The HCAL has an energy resolution of about 10% at 100 GeV for charged pions.

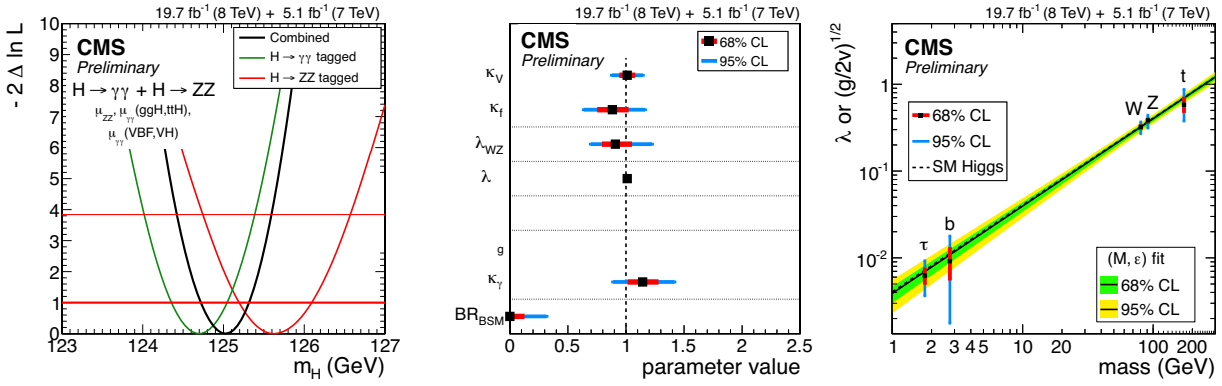

(a) (b) (c)

Figure 2. (a) One dimensional scan of the test statistic versus the hypothesized Higgs boson mass m_H for the $\gamma\gamma$ (green) and $4l$ (red) final states separately and for their combination (black). (b) Summary of the fits for deviations in the coupling for the LHC XS WG benchmark models [5]. For each model, the best fit values of the most interesting parameters are shown, with the corresponding 68% and 95% CL intervals. (c) Summary of the fits for deviations in the coupling using the SM loop induced couplings, expressed as function of the particle mass.

Muons are measured up to $|\eta| < 2.4$ in gas-ionization detectors embedded in the flux-return yoke of the magnet. A full description of the CMS detector can be found in Ref. [1].

Particles in an event are individually identified by the particle-flow reconstruction [2]. This algorithm reconstructs each particle produced in a collision by using an optimised combination of information from the tracker, the calorimeters, and the muon system, and identifies them as either charged hadrons, neutral hadrons, photons, muons, or electrons. Muons are reconstructed by finding compatible track segments in the silicon tracker and the muon detectors [3] and are required to be within $|\eta| < 2.1$. Electron candidates are reconstructed starting from a cluster of energy deposits in the ECAL that is then matched to the momentum associated with a track in the silicon tracker [4].

3 Combination of measurements of properties of the Higgs boson

Following the discovery of a scalar particle at 125 GeV in the ZZ^* and $\gamma\gamma$ channels announced in Ref. [6, 7], the CMS experiment has used the whole datasets collected in 2011 and 2012 to verify in detail that the observed characteristics of that particle are in agreement with the SM predictions for the Higgs boson [8–13]. Results from the combination of several CMS measurements [14] are shown in Fig. 2. The best fit Higgs boson mass as measured in the $\gamma\gamma$ and ZZ^* decay channel is found to be

$$m_H = 125.03\ ^{+0.26}_{-0.27}\ (\text{stat.})\ ^{+0.13}_{-0.15}\ (\text{syst.})\ \text{GeV}$$

where the final detector calibration and alignment are used in the event reconstruction. The precision is dominated by the statistical uncertainty. For the 1D scan of the test statistics as a function of the hypothesized Higgs boson mass shown in Fig. 2a, event yields obtained in the different analyses tagging specific decay modes and production mechanisms are found to be consistent with those expected for the SM Higgs boson. Moreover, the combined best-fit signal strength, relative to the SM expectation, is found to be

$$\mu/\mu_{\text{SM}} = 1.00 \pm 0.09\ (\text{stat.})\ ^{+0.08}_{-0.07}\ (\text{theo.})\ \pm 0.07\ (\text{syst.}).$$

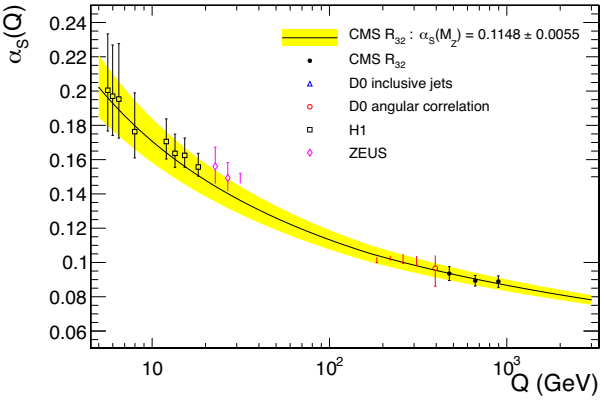

Figure 3. The strong coupling $\alpha_S(Q)$ (solid line) and its total uncertainty (band) evolved from the CMS determination $\alpha_S(M_Z) = 0.1148 \pm 0.0055$ using a 3-loop solution to the RGE as a function of the momentum transfer $Q = \langle p_{T1,2} \rangle$.

In Fig. 2b, fit results of various coupling strength modifiers as defined in Ref. [5] are shown. Best fit values for modifiers of the Higgs coupling to the vector bosons κ_V, the fermions κ_f, the ratio of W boson and Z boson couplings λ_{WZ}, the ratio of couplings to up-type and down-type fermions λ_{du}, the ratio of couplings to leptons and quarks λ_{lq}, the effective gluon coupling κ_g and the total branching into beyond-the-SM channels BR_{BSM} are shown in Fig. 2b. No significant deviation with respect to the SM is found.

Figure 2c shows fits for deviations in the coupling for a generic five-parameter model [14] assuming effective loop couplings according to the SM. For the fermions, the values of the fitted Yukawa couplings are shown, while for vector bosons the square-root of the coupling for the hVV vertex divided by twice the vacuum expectation value of the Higgs boson field is shown. The linear dependence on the mass parameter nicely illustrates the validity of the Higgs mechanism providing the masses of the fundamental particles in the SM.

4 Precision measurements in the SM

4.1 Measurement of α_S using the ratio of the jet cross sections

Besides electroweak symmetry breaking, the most important feature of the SM as a description of the universe at microscopic scales is, arguably, asymptotic freedom. It is a fundamental property of non-abelian gauge theories and predicts that the strong force becomes weaker at short distances or higher momentum transfer. As a stringent test of the energy dependence of α_s according to SM renormalization group equations (RGEs) [15–17], the LEP and HERA experiments have established the validity of the RGEs up to momentum transfers of 208 GeV [18] and the D0 [19] and CDF [20] experiments extended this range up to 400 GeV. The running coupling $\alpha_S(Q)$ can be measured with the ratio of 3-jet to 2-jet cross sections (R_{32}) as a function of the average transverse momentum, $Q = \langle p_{T1,2} \rangle$ of the two leading jets in the event. In this ratio, the dependence on the Dokshitzer–Gribov–Lipatov–Altarelli–Parisi (DGLAP) equations [21–23] governing the parton distribution functions is strongly reduced.

The data sample used in this analysis [24] was collected during 2011 at a proton-proton centre-of-mass energy of 7 TeV corresponding to an integrated luminosity of 5.0 fb^{-1}. For the online event selection, single-jet triggers that reconstruct jets from calorimeter energy deposits are used to select events based on three p_T thresholds, 190, 240, and 370 GeV. Figure 3 shows R_{32} as a function of Q together with results from the H1 [25, 26], ZEUS [27] and D0 [19, 28] experiments. The momentum scale extends from 420 GeV to 1390 GeV. Using a three-loop RGE for $\alpha_s(Q)$, the parameter $\alpha_s(M_Z)$ is

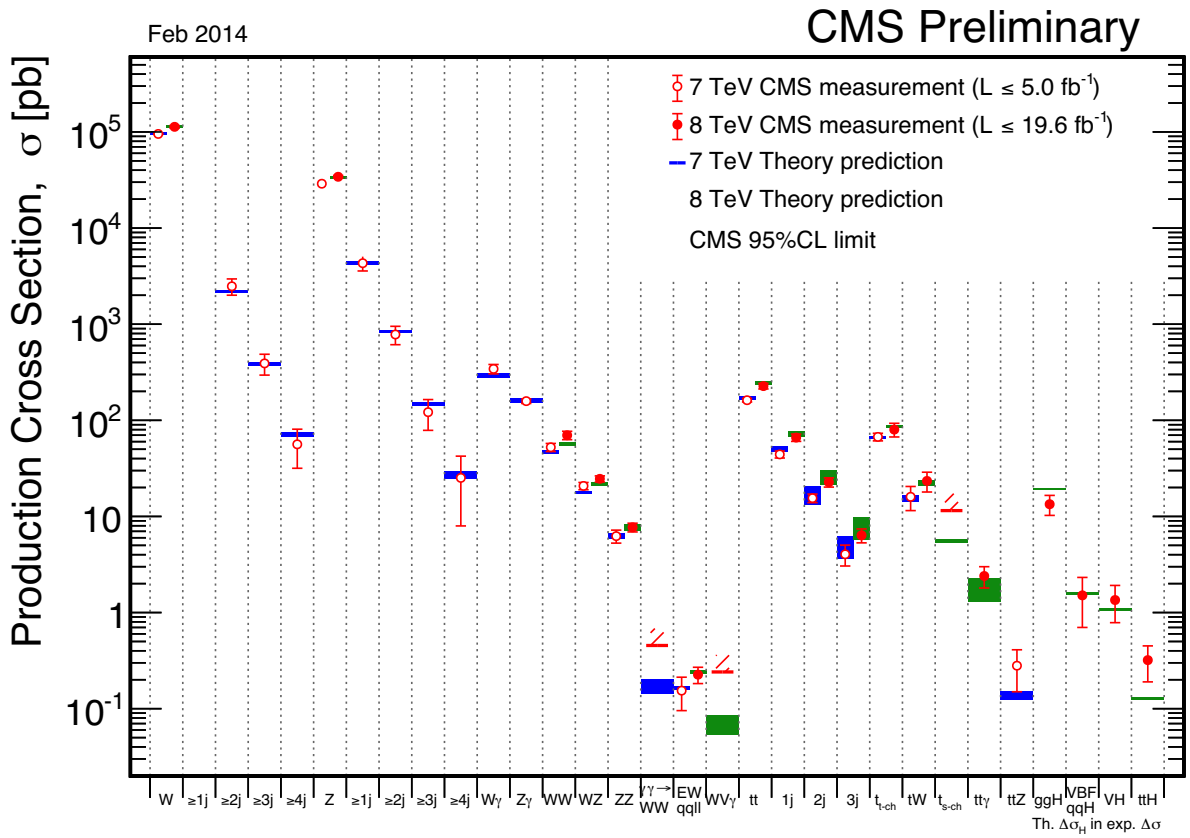

Figure 4. The total production cross section of final states including W and Z bosons, top quarks, and Higgs bosons are compared to theoretical predictions at 7 TeV (blue lines) and 8 TeV (green lines). For single boson production and top quark pair production cross sections of associated jet production with transverse momentum $p_T > 30$ GeV and pseudorapidity $|\eta| < 2.4$ are also shown.

determined to be $\alpha_S(M_Z) = 0.1148 \pm 0.0014\,(\text{exp.}) \pm 0.0018\,(\text{PDF}) \pm 0.0050\,(\text{theory})$ and constitutes the first determination of $\alpha_S(M_Z)$ from measurements at momentum scales beyond 0.6 TeV.

The low uncertainties on α_s are a consequence of a cancellation of the DGLAP evolution of the parton distribution functions in the ratio. This measurement therefore is a stringent test of the evolution of the strong coupling constant at high momentum transfer. No deviation from the expected behaviour is observed.

4.2 Cross section measurements of processes with electroweak bosons

The peculiar gauge structure of the SM predicts a wide range of processes that involve both the strong coupling and the electroweak interactions. Precision cross section measurements of electroweak gauge boson production in association with jets therefore is an ideal testing ground for the SM. The CMS physics programme comprises measurements in many of these final states, some of which have been observed for the first time. Figure 5 shows a summary of single vector boson production in association with jets [29–34], diboson production [35–41], processes involving the fusion of two vector bosons tagged by the presence of two jets with a large rapidity gap [42, 43], single top and top quark

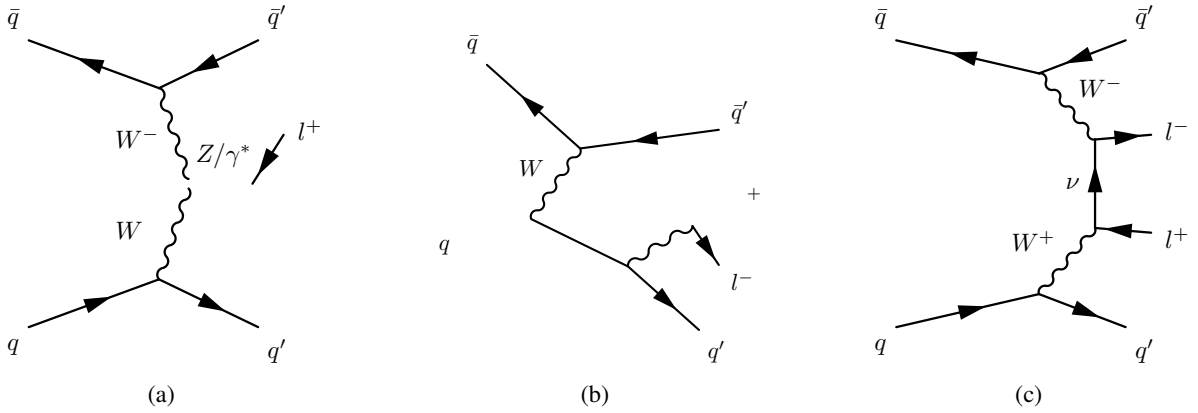

Figure 5. Representative diagrams for dilepton production in association with two jets from pure electroweak processes. Vector boson fusion (left), Bremstrahlung-like (center), and multiperipheral (right) productions.

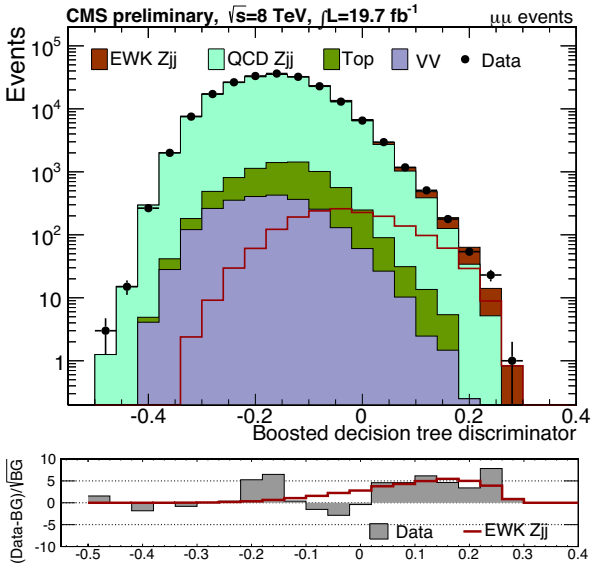

Figure 6. Discriminator shape in the most sensitive region (M_{jj} >750 GeV) for dimuon final states. The total uncertainty from the data-driven background prediction obtained from the photon control sample is shown as a shaded band

pair production in association with jets [44–53] and processes involving the Higgs boson [54–61]. Results are shown for both 7 TeV and 8 TeV measurements.

The distinctive "stairways" pattern in single boson production for different jet multiplicities is understood by noting that the requirement of an additional jet in the tree-level diagram contributes a factor α_s in the Feynman amplitude. It is impossible to discuss all of these results in detail, hence I will focus in the following on the interesting case of a Z boson produced in the fusion of two other vector bosons.

Vector boson fusion production of a Z boson

Besides the mixed electroweak and strong Drell-Yan processes of order $\alpha^2_{EM}\alpha^2_s$, there is also pure electroweak productions of the of order α^4_{EM} predicted in the SM as shown in Fig. 5a. This diagram reveils a hallmark which can be explored experimentally: two jets of very high energy, well separated in pseudo-rapidity and with a large invariant mass, are expected to be produced in association with the

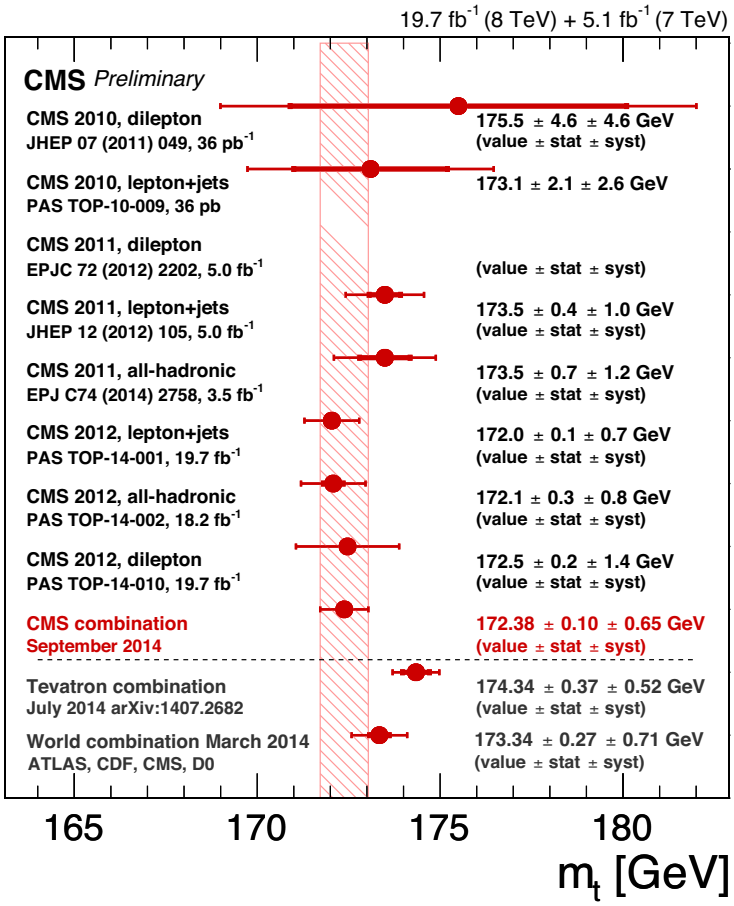

Figure 7. Summary of eight CMS top quark mass measurements and their combination [65]. The precision of the combination corresponds to 0.38%.

dilepton pair from the Z boson [62, 63]. Figure 5(b,c) shows Z-bremsstrahlung processes and multi-peripheral processes, respectively. The evaluation of the corresponding Feynman amplitudes exhibits large negative interferences [63, 64] among the amplitudes of Fig. 5. Therefore, a measurement of this process is both experimentally challenging and an important test of the SM, because the subtle cancellation is easily spoiled by hypothetical effects not accounted for in the SM.

The CMS analysis [43] first selects lepton candidates (electrons or muons) which are well isolated and satisfy $p_T(l) > 20$ GeV. Same-flavor dileptons compatible with $Z \to \mu\mu, ee$ are selected by requiring the dilepton mass to be within 15 GeV of the nominal Z boson mass. At least two jets with $p_T(j) > 50$ GeV are required within the fiducial region $|\eta| < 4.7$. There are two independent analysis carried out. The result shown in Fig. 6 is obtained by a BDT discriminator that is trained on discriminating observables sensitive to the special kinematic configuration. The observables comprise rapidity differences between the Z boson candidate and the jets as well as kinematic variables of the two leading jets. For this discriminator shape, high values of the dijet invariant mass are required and background and signal shapes are used to extract the signal strength from a templated fit to the data. The final result, combining both measurements, is $\sigma = 226 \pm 26$ (stat.) $\pm$ 35 (syst.) fb which is well in agreement with the theoretical value of $\sigma^{\text{th.}} = 239$ fb.

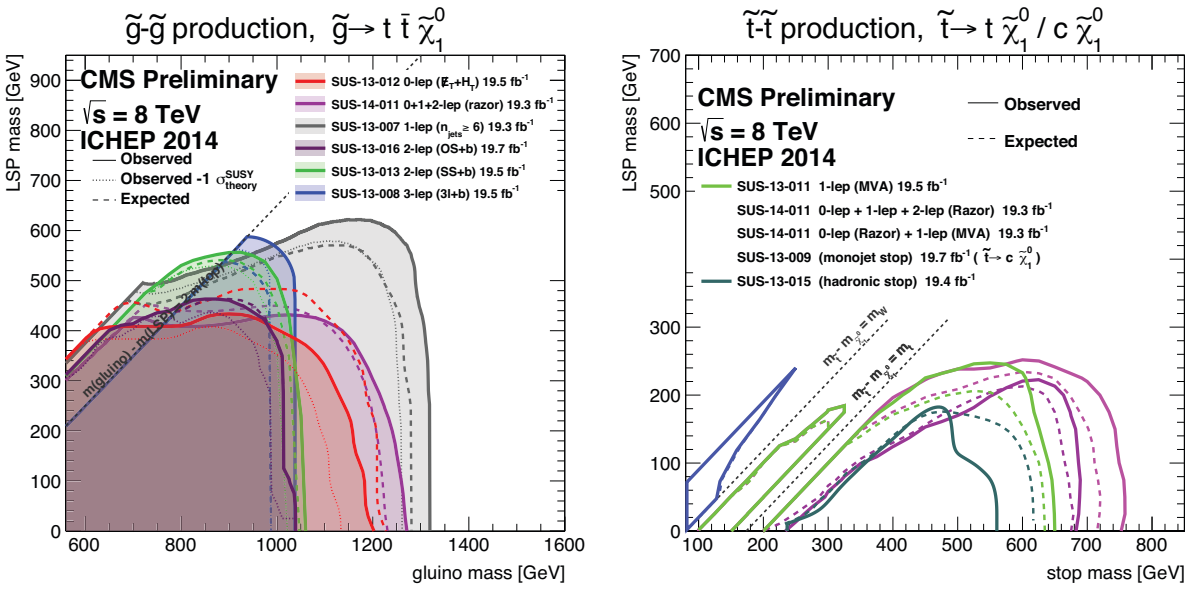

Figure 8. Summary of CMS limits on searches for (a) gluino pair production where each gluino decays into a pair of top squarks and a neutralino and (b) top squark pair prodiction.

4.3 Combination of the top quark mass measurements

Precision measurements of the top quark mass and cross section measurements of single-top and top quark pair production processes are of great interest also because of the special role the top quark plays in various extensions of the SM.

Figure 7 shows the combination of eight separate CMS measurements of the top quark mass [65]. Measurements in the dilepton channel [66–68], the lepton+jets channel [69–71] and the full hadronic channel [72, 73] cover all final states. The measurements [70, 71, 73] perform an in-situ calibration of a global jet energy scale factor using the hadronically decaying W in the top-quark event. This is done in a simultaneous fit of the top-quark and the W boson mass. Thus, the statistical uncertainty from the fit contains a component from the global jet energy scale factor in these cases. The final value of

$$m_t = 172.38 \pm 0.10\ (\text{stat.}) \ \pm 0.65\ (\text{syst.})\ \text{GeV}$$

corresponds to a precision of 0.38% which is a remarkable achievement.

5 Searches for supersymmetry

Supersymmetry (SUSY) is an extension of the standard model (SM) which proposes a superpartner for each SM particle [74–79] in order to mitigate the virtual contributions of the SM particles to the self energy of the Higgs boson by contributions with opposite sign. This cancellation reduces the need for large fine tuning in the Higgs boson mass calculation [80, 81]. An appealing feature of many models with SUSY is that the lightest supersymmetric particle (LSP) is stable and a viable dark matter candidate [82, 83]. Many searches therefore require a large imbalance in the total transverse momentum ($E_{\mathrm{T}}^{\mathrm{miss}}$).

Since the top quark has the largest contribution to the Higgs boson self energy, the superpartner of the top quark must be light in order to avoid unnaturally large fine-tuning. A similar argument

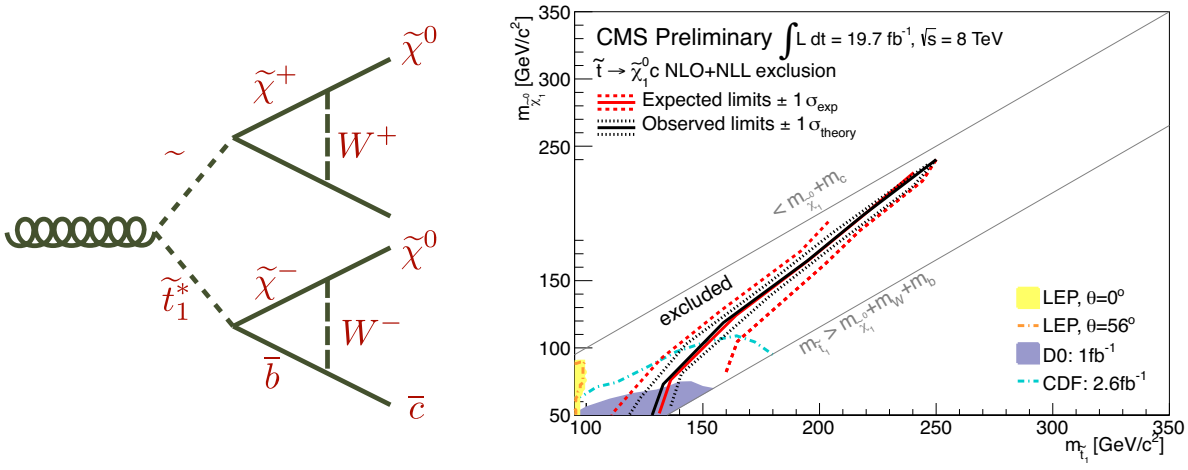

Figure 9. (a) Diagram for the pair production of top squarks with the decay mode $\tilde{t}_1 \to c + \tilde{\chi}_1^0$. (b) Observed and expected $\pm 1\sigma$ limits on top squark production cross section in the $\tilde{t}_1, \tilde{\chi}_1^0$ mass plane [86].

holds for the gluino, because it contributes to the top squark self-energy. One prediction of these "natural" models with a spectacular experimental signature is pair production of gluinos decaying through top squarks to an LSP that is assumed to be stable and only weakly interacting. Moreover, direct top squark pair production is predicted at a high rate. Recent searches, summarized in Fig. 8, have excluded light top squarks up to 600-700 GeV and gluinos up to 1.3 TeV.

A new development in this context aims to evade one important restriction pertaining to these results: They are often obtained under the assumption of a large mass difference between the initial strongly produced SUSY particle and the LSP. However, if the mass of the LSP is very close to the parent SUSY particle, almost all of the momentum of the parent SUSY particle is carried by the LSP and the searches with a requirement for large $E_{\mathrm{T}}^{\mathrm{miss}}$ are not sensitive. Moreover, any decay products of the SUSY particles will fall short of reconstruction thresholds.

An important example is a model with a top squark and a nearly degenerate LSP that leads to a flavour violating loop induced decay as shown in Fig. 9a. Similar mass configurations have been proposed to reconcile measurements of the dark matter relic density with theoretical predictions of models with SUSY [84, 85]. By exploiting the fact that the initial strongly interacting partons may radiate off another high energetic parton (initial-state radiation, ISR) that is reconstructed as a jet, this model can be tested without the assumption of large $E_{\mathrm{T}}^{\mathrm{miss}}$ coming from the LSPs. In consequence, the event topology considered in Ref. [86] is a monojet signature. The jets from the charm quarks are assumed to be too soft to be reconstructed. An important irreducible background in this search is $Z \to \nu\nu$ which can be estimated using $Z \to \mu\mu$ control regions. Figure 9b shows the result in the parameter plane spanned by the top squark mass and the LSP mass. Top squarks that are nearly degenerate with the LSP are excluded at 95% CL up to approx. 250 GeV.

6 Summary

The CMS experiment has used the proton-proton collision data collected during the 2011 and 2012 runs of the Large Hadron Collider to produce a large number of groundbreaking results in precision measurements of standard model observables and in searches for new physics. The discovery of the

Higgs boson is certainly among the most prominent results and the mass measurement combining $\gamma\gamma$ and $4l$ channels results in $m_H = 125.03\ ^{+0.26}_{-0.27}$ (stat.) $^{+0.13}_{-0.15}$ (syst.) GeV. The low systematic uncertainty is a testimonial of the change in focus from discovery to precision measurements and even first constraints of new physics in the Higgs sector have been obtained.

Many further measurements in the electroweak sector are also in agreement with predictions from the SM. Cross sections of processes involving large negative interference like the fusion of two vector bosons have been measured and provide stringent tests of the SM.

Various extensions of the SM are furthermore tested by searching for signals of decays of SUSY particles. Tight limits on the production of gluinos and top squarks have been obtained. No convincing evidence for a deviation has been found so far. Important loopholes like the case of SUSY particles with degenerate spectra are successivly closed.

Acknowledgements

We wish to congratulate our colleagues in the CERN accelerator departments for the excellent performance of the LHC machine. We thank the technical and administrative staff at CERN and other CMS institutes, and acknowledge support from: FMSR (Austria); FNRS and FWO (Belgium); CNPq, CAPES, FAPERJ, and FAPESP (Brazil); MES (Bulgaria); CERN; CAS, MoST, and NSFC (China); COLCIENCIAS (Colombia); MSES (Croatia); RPF (Cyprus); Academy of Sciences and NICPB (Estonia); Academy of Finland, ME, and HIP (Finland); CEA and CNRS/IN2P3 (France); BMBF, DFG, and HGF (Germany); GSRT (Greece); OTKA and NKTH (Hungary); CSIR, DAE, and DST (India); IPM (Iran); SFI (Ireland); INFN (Italy); NRF (Korea); LAS (Lithuania); CINVESTAV, CONACYT, SEP, and UASLP-FAI (Mexico); PAEC (Pakistan); SCSR (Poland); FCT (Portugal); JINR (Armenia, Belarus, Georgia, Ukraine, Uzbekistan); MST and MAE (Russia); MSTDS (Serbia); MICINN and CPAN (Spain); Swiss Funding Agencies (Switzerland); NSC (Taipei); TUBITAK and TAEK (Turkey); STFC (United Kingdom); DOE and NSF (USA).

References

[1] CMS Collaboration, JINST **3**, S08004 (2008)
[2] CMS Collaboration, Tech. Rep. CMS-PAS-PFT-09-001 (2009)
[3] CMS Collaboration, Tech. Rep. CMS-PAS-MUO-10-002 (2010)
[4] CMS Collaboration, Tech. Rep. CMS-PAS-EGM-10-004 (2010)
[5] S. Heinemeyer et al. (LHC Higgs Cross Section Working Group) (2013), 1307.1347
[6] ATLAS Collaboration, Phys.Lett. **B716**, 1 (2012), 1207.7214
[7] CMS Collaboration, Phys.Lett. **B716**, 30 (2012), 1207.7235
[8] F. Englert, R. Brout, Phys.Rev.Lett. **13**, 321 (1964)
[9] P.W. Higgs, Phys.Lett. **12**, 132 (1964)
[10] P.W. Higgs, Phys.Rev.Lett. **13**, 508 (1964)
[11] G. Guralnik, C. Hagen, T. Kibble, Phys.Rev.Lett. **13**, 585 (1964)
[12] P.W. Higgs, Phys.Rev. **145**, 1156 (1966)
[13] T. Kibble, Phys.Rev. **155**, 1554 (1967)
[14] CMS Collaboration, Tech. Rep. CMS-PAS-HIG-14-009, CERN, Geneva (2014)
[15] J. Callan, Curtis G., Phys.Rev. **D2**, 1541 (1970)
[16] K. Symanzik, Commun.Math.Phys. **18**, 227 (1970)
[17] K. Symanzik, Commun.Math.Phys. **23**, 49 (1971)

[18] P.D. Group (Particle Data Group), Phys. Rev. D **86**, 010001 (2012)
[19] D0 Collaboration, Physics Letters B **718**, 56 (2012)
[20] CDF Collaboration, Phys. Rev. Lett. **88**, 042001 (2002)
[21] V. Gribov, L. Lipatov, Sov.J.Nucl.Phys. **15**, 438 (1972)
[22] G. Altarelli, G. Parisi, Nucl.Phys. **B126**, 298 (1977)
[23] Y.L. Dokshitzer, Sov.Phys.JETP
[24] CMS Collaboration, Eur.Phys.J. 1304.7498
[25] H1 Collaboration, The European Physical Journal C **65**, 363 (2010)
[26] H1 Collaboration, The European Physical Journal C **67**, 1 (2010)
[27] ZEUS Collaboration, Nuclear Physics B **864**, 1 (2012)
[28] D0 Collaboration, Phys. Rev. D **80**, 111107 (2009)
[29] CMS Collaboration, JHEP **1110**, 132 (2011), 1107.4789
[30] CMS Collaboration, Phys.Rev.Lett. **112**, 191802 (2014), 1402.0923
[31] CMS Collaboration, JHEP **1201**, 010 (2012), 1110.3226
[32] CMS Collaboration, Tech. Rep. CMS-PAS-SMP-12-023, CERN, Geneva (2014)
[33] CMS Collaboration, JHEP **1402**, 013 (2014), 1310.1138
[34] CMS Collaboration, Phys.Lett. **B735**, 204 (2014), 1312.6608
[35] CMS Collaboration, Eur.Phys.J. **C73**, 2283 (2013), 1210.7544
[36] CMS Collaboration, Eur.Phys.J. **C73**, 2610 (2013), 1306.1126
[37] CMS Collaboration, Phys.Lett. **B721**, 190 (2013), 1301.4698
[38] CMS Collaboration, Tech. Rep. CMS-PAS-SMP-12-006, CERN, Geneva (2013)
[39] CMS Collaboration, JHEP **1301**, 063 (2013), 1211.4890
[40] CMS Collaboration, Tech. Rep. CMS-PAS-SMP-13-005, CERN, Geneva (2013)
[41] CMS Collaboration, JHEP **1307**, 116 (2013), 1305.5596
[42] CMS Collaboration, JHEP **1310**, 062 (2013), 1305.7389
[43] Tech. Rep. CMS-PAS-FSQ-12-035, CERN, Geneva (2013)
[44] CMS Collaboration, Phys.Rev.Lett. **110**, 172002 (2013), 1303.3239
[45] CMS Collaboration, Tech. Rep. CMS-PAS-TOP-13-011, CERN, Geneva (2014)
[46] CMS author, Tech. Rep. CMS-PAS-TOP-13-009, CERN, Geneva (2013)
[47] CMS Collaboration, Tech. Rep. CMS-PAS-TOP-12-040, CERN, Geneva (2013)
[48] CMS Collaboration, Phys.Rev.Lett. **110**, 022003 (2013), 1209.3489
[49] CMS Collaboration, Tech. Rep. CMS-PAS-TOP-12-011, CERN, Geneva (2012)
[50] CMS Collaboration, JHEP **1212**, 035 (2012), 1209.4533
[51] CMS Collaboration, Tech. Rep. CMS-PAS-TOP-12-041, CERN, Geneva (2013)
[52] CMS Collaboration, Tech. Rep. CMS-PAS-TOP-12-007, CERN, Geneva (2012)
[53] JHEP **1211**, 067 (2012), 1208.2671
[54] CMS Collaboration, Tech. Rep. CMS-PAS-HIG-13-005, CERN, Geneva (2013)
[55] CMS Collaboration, Tech. Rep. CMS-PAS-HIG-13-015, CERN, Geneva (2013)
[56] CMS Collaboration, Tech. Rep. CMS-PAS-HIG-13-019, CERN, Geneva (2013)
[57] CMS Collaboration, Tech. Rep. CMS-PAS-HIG-13-020, CERN, Geneva (2013)
[58] CMS Collaboration, Tech. Rep. CMS-PAS-SMP-13-002, CERN, Geneva (2013)
[59] CMS Collaboration, Phys. Rev. D **84**, 052011 (2011)
[60] CMS Collaboration, JHEP **1406**, 009 (2014), 1311.6141
[61] CMS Collaboration, JHEP **2012** (2012)

[62] D.L. Rainwater, R. Szalapski, D. Zeppenfeld, Phys.Rev. **D54**, 6680 (1996), hep-ph/9605444
[63] V. Khoze, M. Ryskin, W. Stirling, P. Williams, Eur.Phys.J. **C26**, 429 (2003), hep-ph/0207365
[64] C. Oleari, D. Zeppenfeld, Phys.Rev. **D69**, 093004 (2004), hep-ph/0310156
[65] CMS Collaboration, Tech. Rep. CMS-PAS-TOP-14-015, CERN, Geneva (2014)
[66] CMS Collaboration, JHEP **1107**, 049 (2011), 1105.5661
[67] CMS Collaboration, Eur.Phys.J. 1209.2393
[68] CMS Collaboration, Tech. Rep. CMS-PAS-TOP-14-010, CERN, Geneva (2014)
[69] CMS Collaboration, Tech. Rep. CMS-PAS-TOP-10-009 (2011)
[70] CMS Collaboration, JHEP **1212**, 105 (2012), 1209.2319
[71] CMS Collaboration, Tech. Rep. CMS-PAS-TOP-14-001, CERN, Geneva (2014)
[72] CMS Collaboration, Eur.Phys.J. **C74**, 2758 (2014), 1307.4617
[73] CMS Collaboration, Tech. Rep. CMS-PAS-TOP-14-002, CERN, Geneva (2014)
[74] S. Martin (1997), , hep-ph/9709356
[75] J. Wess, B. Zumino, Nucl. Phys **B 70**, 39 (1974)
[76] H.P. Nilles, Phys. Reports **110**, 1 (1984)
[77] H.E. Haber, G.L. Kane, Phys. Reports **117**, 75 (1987)
[78] R. Barbieri, S. Ferrara, C.A. Savoy, Phys. Lett. **B119**, 343 (1982)
[79] S. Dawson, E. Eichten, C. Quigg, Phys. Rev. **D31**, 1581 (1985)
[80] E. Witten, Nucl. Phys. **B 188**, 513 (1981)
[81] S. Dimopoulos, H. Georgi, Nucl. Phys. **B 193**, 150 (1981)
[82] G.R. Farrar, P. Fayet, Phys.Lett. **B76**, 575 (1978)
[83] J.R. Ellis, J.S. Hagelin, D.V. Nanopoulos, K.A. Olive, M. Srednicki, Nucl. Phys. **B238**, 453 (1984)
[84] S.P. Martin, Phys.Rev. **D75**, 115005 (2007), hep-ph/0703097
[85] S.P. Martin, Phys.Rev. **D76**, 095005 (2007), 0707.2812
[86] CMS Collaboration, Tech. Rep. CMS-PAS-SUS-13-009, CERN, Geneva (2014)